Soliton Dynamics in Mode-Locked Lasers

S.T. Cundiff

JILA, National Institute of Standards and Technology and University of Colorado, Boulder, CO 80309-0440 USA
cundiffs@jila.colorado.edu

Mode-locked lasers generate ultra-short optical pulses, with durations ranging from hundreds of picoseconds (ps) down to a few femtoseconds (fs). The pulse circulating in the cavity of a mode-locked laser can be thought of as a dissipative soliton, where the dissipation is due to the inevitable presence of loss, which must be compensated by gain. In addition to gain and loss, the pulse experiences nonlinearity and dispersion, the key ingredients for any soliton system. These effects occur in physical elements that do not completely fill the cavity, thus there is a similarity to the dispersion management that is used in telecommunications systems.

There are a number of features that make a mode-locked laser an excellent system for experimental study of soliton dynamics. Since a pulse is emitted once per round trip, it is possible to watch the evolution of the pulse. Furthermore, an essentially infinite propagation distance can be observed. There are no variations in the parameters from round-trip to round-trip, which makes simulation easier, although it does restrict the applicability of the results to real telecommunications systems, which can display statistical variations. It is possible to examine parameter regimes that are not easily accessible otherwise, for example peak power or characteristic nonlinear or dispersion lengths. And finally, it is relatively easy to make a change of parameters for the entire propagation distance at once.

In this chapter, the basics of mode-locked lasers will be presented first. Then the experimental observation of polarization evolution in a mode-locked fiber laser, which demonstrated both the presence of polarization-locked vector solitons and instability of the fast axis, will be discussed. This will be followed by a section on soliton instabilities, dubbed "exploding solitons", in a mode-locked Ti:sapphire laser. The next section summarizes the recent advances on phase control of mode-locked lasers, which brings up interesting new issues regarding how nonlinearity impacts both the group and phase velocities inside the laser cavity.

1 Mode-Locked Laser Basics

A laser is essentially an optical oscillator and, as such, requires the two basic constituents of any oscillator, namely amplification and feedback. The

S.T. Cundiff: *Soliton Dynamics in Mode-Locked Lasers*, Lect. Notes Phys. **661**, 183–206 (2005)
www.springerlink.com

amplification is provided by stimulated emission in a gain medium. Feedback is provided by the laser "cavity", which is a set of mirrors that cause the light to reflect back on itself. One of the mirrors, called the output coupler, transmits a small fraction of the incident light to provide output [1].

The word "mode-locked" refers to the frequency domain description of how ultra-short pulses are generated by a laser. The requirement that the electromagnetic field be unchanged after one round trip in the laser means that lasing only occurs for frequencies such that the cavity length is an integer number of wavelengths. These are referred to as the longitudinal modes and occur at frequencies $\nu_j = jc/2nl$, where j is an integer that indexes the modes, c is the speed of light, n is the average index of refraction in the cavity and l is the cavity length. If multiple modes lase at the same time, then a short pulse can be formed, but only if the modes are locked in phase, i.e., the laser is mode-locked. As illustrated in Fig. 1, this actually produces a pulse train, where the time between pulses equals the cavity round trip time. It should be noted that there are others types of lasers that generate pulses, the most common being called a "q-switched" laser. However, the pulse evolution in those lasers is unrelated to soliton dynamics. Non-pulsed lasers are designated as "continuous wave" (CW).

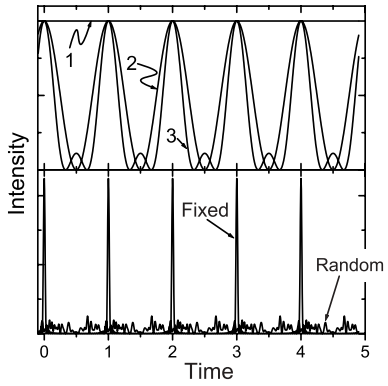

Fig. 1. Formation of a pulse train due to constructive interference among longitudinal modes. The intensities, $I(t) = |E(t)|^2$ for one, two and three longitudinal modes are shown in the *upper* panel. The *lower* panel shows 30 modes for both fixed phases, i.e., mode-locked, and random phases

Despite the fact that the term "mode-locking" comes from the frequency domain description, the dynamics are typically described in the time domain. The key element, which distinguishes mode-locked lasers from other lasers, is the presence of an element in the cavity that causes it to modelock. This can be an active element, essentially a shutter that is opened once per round trip by an external drive (active mode-locking), or a passive element, in which

case the pulse itself causes it to "open" [2]. The latter case of passive mode-locking produces the shortest pulses. Passive mode-locking can be described in terms of a saturable absorber, i.e., one where the absorption saturates, so that a higher intensity is less attenuated than a lower intensity. This could be a due to a real absorber, such as dye molecules or a semiconductor, or it could be virtual. A virtual saturable absorber generally relies on the Kerr effect, which means that the index of refraction depends on intensity, $n = n_0 + n_2 I$ where n_0 is the linear index of refraction, n_2 is the Kerr coefficient and I is the intensity.

A schematic diagram showing the elements present in a mode-locked laser is shown in Fig. 2. Note that the different elements are not necessarily distinct, as shown in the figure, for example the gain medium often is also dispersive and nonlinear. Additionally, loss is not specifically shown; the output coupler causes loss and there maybe some loss in the other elements. As implied by the discrete elements, the various effects typically are not spread throughout the cavity, but rather only occur for a sub-section of it. This suggests a connection with dispersion management in telecommunications, which indeed has been applied to mode-locked lasers [3].

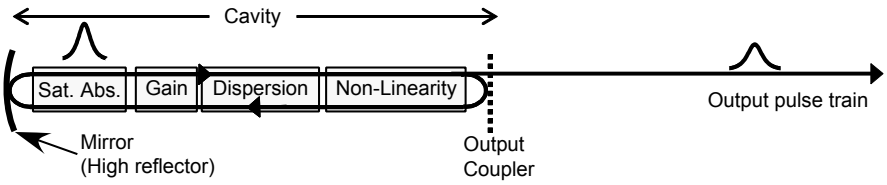

Fig. 2. Block diagram showing the essential elements of a mode-locked laser

Thus all of the physical processes associated with dissipative solitons are present in mode-locked lasers. Saturable absorption, which is also a dissipative process, is present. In the steady state, the gain medium in a laser is strongly saturated, hence gain saturation must be considered as well. In addition, birefringence, which means that the index of refraction is not a scalar but rather a tensor, may be present as well. This can cause the polarization state to evolve with propagation.

2 Soliton Polarization Evolution

Optical fiber is the most common medium for studying temporal optical solitons. This has been strongly motivated by the application to telecommunications. A key technology for optical telecommunications is the erbium-doped fiber amplifier (EDFA) [4]. The erbium dopant atoms provide gain to amplify optical signals that are attenuated due to loss in the transmission fiber. Naturally, this gain medium can also be used to construct a laser. Figure 3 shows

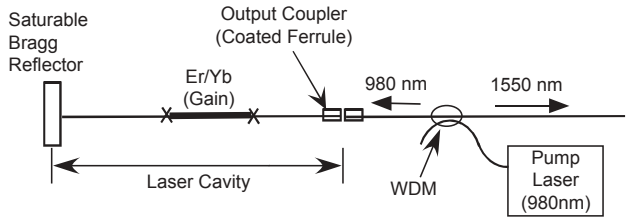

Fig. 3. Diagram of mode-locked fiber laser

a schematic of a mode-locked fiber laser that uses a saturable Bragg reflector (SBR) for mode-locking [5]. This laser uses a section of fiber co-doped with erbium (Er) and ytterbium (Yb) for gain. The gain fiber is pumped by a 980 nm diode laser, which enters the cavity through the output coupler. The wavelength division multiplexer (WDM) separates the pump light from the 1550 nm laser emission. The remainder of the cavity is made up of standard telecommunications fiber (simply called "single mode fiber" or SMF), which has anomalous dispersion at 1550 nm, whereas the gain fiber has normal dispersion. The output coupler, which is a mirror coated directly onto a cleaved fiber, serves as one end of the cavity. The other end is the SBR, which is a monolithic semiconductor structure combining a mirror and a single quantum well, which provides saturable absorption. The quantum well provides "real" saturable absorption and thus has a finite life time, as opposed to the more common fiber lasers that use nonlinear polarization to mode-lock [6].

Hasegawa and Tappert predicted the existence of temporal solitons in optical fiber in 1973 [7]. This pioneering paper ignored the fact that all "single" mode optical fiber actually supports two orthogonal polarization modes; the term "single" mode refers only to the transverse profile. If optical fiber were perfectly isotropic, the polarization modes would be completely degenerate and this treatment would be correct. In reality, manufacturing imperfections, externally applied stress, or bending lifts the degeneracy between the modes. Thus fiber supports two orthogonally-polarized modes with differing propagation constants; i.e., fiber is birefringent [8]. The experimental observation of optical solitons [9] and the subsequent explosion of work [10] proved that this omission was nevertheless justified in many circumstances.

The difference in phase velocities of the two modes causes the polarization state of a pulse to evolve as it propagates. In general, the group velocities are also unequal. The differing group velocities result in temporal pulse splitting, a phenomenon known as polarization mode dispersion and currently of great concern for non-soliton long distance optical communication systems [11]. The differing group velocities might also be expected to prevent the formation of a soliton with energy in both orthogonal polarization modes (i.e., along both principal axes of the birefringence). However solitons are remarkably robust; they do exist under these conditions and propagate as a unit [12]. To cancel

the group velocity difference, the orthogonally-polarized components of the soliton shift their center frequency slightly. This phenomenon has been described theoretically using a pair of coupled non-linear Schrödinger equations [13]. Since the phase velocities are still different, the polarization state evolves with propagation.

A "vector soliton" is a multi-dimensional entity that propagates in an invariant or periodic manner in an environment that is destructive in the absence of compensating nonlinearity [14]. The situation described above can be denoted as a "group-velocity-locked vector soliton" as it has some amplitude on both principal axes and is therefore multi-dimensional.

Prior to their observation in a fiber laser [15], states that also display locking of the phase velocities, in addition to the group velocities, had only been characterized theoretically [16, 17, 18, 19, 20, 21]. These states are elliptically-polarized and they exist due to a dynamic balance between linear and nonlinear birefringence. The nonlinear birefringence arises from a combination of self and cross phase-modulation. Figure 4 shows a schematic comparison between just linear birefringence [Fig. 4a] and the balance that can occur when nonlinear processes are included [Fig. 4b]. Coherent energy coupling (also called four-wave-mixing) provides a stabilizing mechanism that maintains the exact power distribution for the balance to occur. These states are designated "polarization-locked vector solitons" (PLVS) as they have power along both principal axes, and thus are multi-dimensional.

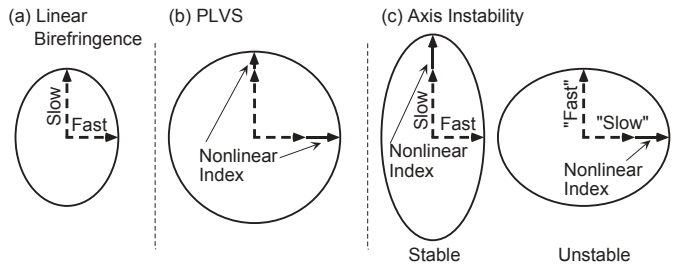

Fig. 4. Schematic of the interplay between linear and nonlinear birefringence. (**a**) Linear birefringence alone; (**b**) balance between linear and nonlinear birefringence that occurs for a PLVS; (**c**) conditions for the fast axis instability. Note that, in (**c**), the axes are labeled by their net birefringence due to both linear and nonlinear contributions. The ellipses are an aid for visualizing the relative magnitude of the indices of refraction

In addition to the PLVS, states with fixed linear polarization are also observed in the fiber laser. These occur at larger values of birefringence than the PLVS and occur due to axis instabilities [22, 23, 24]. Axis instabilities arise when the nonlinear birefringence can cause the phase velocity of the

fast axis to become comparable to, or slower than, that of the slow axis [see Fig. 4c]. In this case, the fast axis becomes unstable.

The first observation showed that the polarization state in a fiber laser could spontaneously lock, although the mechanisms were unclear [25]. This triggered theoretical work to show that the PLVS, predicted for strictly conservative systems [16, 17, 18, 19, 20, 21], could exist in the non-conservative, i.e., dissipative, environment of a fiber laser [26]. Based on this theoretical work, it was possible to positively identify the polarization-locked states that were occurring [15, 27, 28].

2.1 Theoretical Background

The full vector model describing the propagation of the two components polarized along the orthogonal principal axes of a lossless fiber are given by the conservative coupled nonlinear Schrödinger equations (CNLSE) [13, 29, 30]:

$$\mathrm{i}\frac{\partial u}{\partial z} + \mathrm{i}\delta\frac{\partial u}{\partial t} + \gamma u + \frac{1}{2}\frac{\partial^2 u}{\partial t^2} + (|u|^2 + A|v|^2)u + Bv^2u^* = 0\,, \tag{1}$$

$$\mathrm{i}\frac{\partial v}{\partial z} - \mathrm{i}\delta\frac{\partial v}{\partial t} - \gamma v + \frac{1}{2}\frac{\partial^2 v}{\partial t^2} + (|v|^2 + A|u|^2)v + Bu^2v^* = 0\,, \tag{2}$$

where u and v are the component envelopes along the slow and fast axes respectively, z and t are the normalized time and distance, 2δ and 2γ are the normalized group and phase velocity differences, and A and B are the cross phase modulation (XPM) and coherent energy exchange coefficients, respectively.

These equations admit two linearly-polarized fundamental soliton solutions:

$$\begin{aligned} u(t,z) &= u_0\mathrm{sech}(t-\delta z)\exp(\mathrm{i}\gamma z) \quad & v(t,z) &= 0 \\ u(t,z) &= 0 & v(t,z) &= v_0\mathrm{sech}(t+\delta z)\exp(\mathrm{i}\gamma z)\,. \end{aligned} \tag{3}$$

For an isotropic and conservative medium, $B = 1 - A$ in 1 and 2. When $A = 1$ [the self phase modulation (SPM) and XPM coefficients are equal, and the coherent energy exchange vanishes] and $\delta = 0$, the CNLSE are integrable, with stationary phase-locked solutions [31]. The experimental observation of these simple hyperbolic secant shaped solutions, known as "Manakov" solitons, is difficult, since $A \neq 1$ for most low-loss materials. Through engineering of the SPM and XPM coefficients in an anisotropic waveguide ($A \sim 0.95$), spatial "Manakov" solitons have been observed [32]. Spatial solitons are governed by CNLSE analogous to 1 and 2. In isotropic media such as standard single mode fiber, $A = 2/3$ and rigorous temporal "Manakov" solitons cannot occur.

If the linear birefringence is significantly larger than the nonlinear birefringence, then the relative optical phase between components varies so rapidly

that all phase-dependent phenomena effectively average to zero on propagation [13]. Thus, the coherent energy coupling and phase velocity difference terms in 1 and 2 can be ignored, resulting in the fact that coupling between the two components will only be due to incoherent cross-phase modulation. In this case, the solutions approximate "Manakov" solitons. This condition is designated "high birefringence." It occurs in SMF if the peak power is less than 1 W, or in polarization-maintaining fiber, which has very large birefringence intentionally manufactured into it. For high birefringence, the solutions to 1 & 2 correspond to two orthogonally-polarized pulses along the birefringent axes that mutually trap each other. They propagate as a non-dispersing group velocity-locked vector soliton [13, 14]. The cross-phase modulation causes the central optical frequency of one component to increase and the other to decrease. In conjunction with a frequency-dependent group velocity, these shifts equalize their group velocities [13]. In the absence of nonlinearity (i.e., cross-phase modulation), the components retain their central frequencies and travel at unequal group velocities; this causes them to split temporally. Due to the large phase velocity difference between the components, the polarization state of this vector soliton evolves rapidly with propagation. At any given point, the same polarization state applies to the entire pulse because the two components have the same amplitude and phase profiles [33]. Standard soliton communications systems operate in this high birefringence regime and utilize group velocity-locked vector solitons. Hence, these soliton systems are relatively immune to the detrimental pulse splitting effects of random and unequal group velocities (polarization mode dispersion) that often impair the performance of non-soliton communications systems [11, 34].

The designation "low birefringence" means that the linear and nonlinear birefringence are comparable (the latter depends on polarization state). In this case, the difference between group velocities can typically be ignored. The two polarization components are now coherently coupled, and the relative optical phase, phase velocity differential, and coherent energy exchange between the orthogonal polarization components must be retained. Theoretical analysis has found three lowest-order stationary solutions for the low birefringence case: two fundamental soliton solutions that are linearly-polarized along either the fast or slow axis (3) , and a (numerical) elliptically- polarized solution [18, 19, 20]. The elliptically- polarized solution is a PLVS because it contains energy in both components and propagates without change in its polarization state. The components have a relative phase of $\pm\pi/2$, but do not necessarily have amplitude profiles of the same functional shape. Hence, the polarization state is not uniform across the pulse [18, 19, 20]. Other higher-order stationary solutions have also been found [14, 16, 19]. The elliptically-polarized solitons possess a weak oscillatory instability, in contrast to solitons that are linearly-polarized along the fast axis, which are unstable [23].

For a PLVS to survive propagation with a constant polarization state, the phase velocities of the two components must be identical. As shown in Fig. 4b, a nonlinear index difference is created by an unequal distribution of energy between the two axes. The resulting difference (or nonlinear birefringence) in the nonlinear index compensates the linear birefringence exactly. This means that the phase velocities of the two axes are identical.

The magnitude of the nonlinear birefringence depends on the difference between the intensities of the components, i.e., the ellipticity of the polarization state, since the relative phases must be $\pm\pi/2$. Thus, the ellipticity of the polarization state depends directly on the linear birefringence. Within the approximation of equal component profiles, this can be expressed as

$$|V|^2 - |U|^2 = \frac{\gamma}{g}\,, \tag{4}$$

where U and V are the time integrated amplitudes of u and v, $g \approx q(1-A)$, and q is a soliton parameter that is inversely proportional to the soliton period and proportional to the square of the pulse energy [17, 18]. Equation 4 also shows that $|V|^2 \geq |U|^2$ with the component along the fast axis possessing greater intensity. The magnitude of the nonlinear birefringence of a pulse is limited by its energy and width (implicitly here through normalization) such that a PLVS cannot exist for linear birefringence $\gamma > (|V|^2 + |U|^2)g$. Equivalently, this limit occurs as $|U|^2 \to 0$ and the polarization state approaches linear polarization along the fast axis.

For large values of linear birefringence, a soliton that is linearly-polarized along the fast axis (second line in 3) becomes unstable. Instability of the fast axis due to nonlinearity was first described for CW propagation [22]. It also occurs for solitons [23], and has been carefully addressed using soliton perturbation theory [18]. Because the fast axis is unstable, a pulse that is initially polarized along it will evolve away from it towards the slow axis, which is a stable point, and typically will undergo oscillations around it. Because the fiber laser is non-conservative, the oscillations are damped, resulting in solitons that are linearly-polarized along the slow axis. The role played by nonlinearity provides an important distinction between the fast axis instability and the PLVS. In absence of nonlinearity, the PLVS states are not stable and do not exist, i.e., nonlinearity creates a new state. In contrast, nonlinearity destroys the stability of the fast axis, with the result that there is only a single stable state (the slow axis).

2.2 Experiment

Measurements have been performed on several implementations of the fiber laser with essentially identical results; the details vary from laser to laser (mainly the fiber lengths). Typical output optical spectra are shown in Fig. 5. The clean sech^2 spectrum shows that soliton-like pulse shaping dominates the

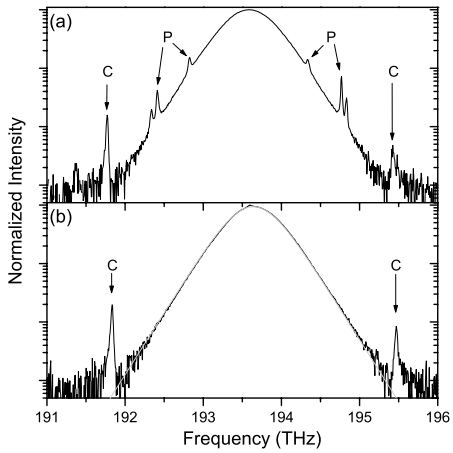

Fig. 5. Optical spectrum of the fiber laser output for (**a**) non-polarization-locked and (**b**) polarization-locked operation. The side-bands marked "C" are due to the periodic perturbation by the cavity, while those marked "P" are due to periodic perturbation of the polarization. In (**b**), the *gray* line shows a fit to a hyperbolic secant spectrum

characteristics of the pulse. The pulse width can be adjusted by changing the pulse energy.

The soliton period, assuming a linearly-polarized pulse, is given by [29]

$$z_0 = \frac{\tau_0^2}{2|\beta_2|} \tag{5}$$

where τ_0 is the pulse width and β_2 is the GVD. For the shortest pulses (350 fs), $z_0 = 3.5$ m, i.e., approximately the round-trip length of the cavity. For the longest pulses, $z_0 = 20$ m. Periodic perturbations to a soliton cause side-bands in the optical spectrum, due to phase- matching of the radiation shed by the soliton as it adjusts after being perturbed [35, 36]. The side-bands marked by "C" in Fig. 5 are due to the periodic perturbation by the cavity (the side-bands designated by "P" will be discussed later). Their relatively small magnitude (<0.1% of total energy) shows that the soliton is not strongly perturbed as it circulates in the cavity.

The linear birefringence in the cavity is controlled by wrapping a portion of the cavity fiber around two 5.5 cm diameter disks (known as fiber polarization controller paddles) [37]. Each disk has three wraps, which for standard single mode fiber, provides approximately $\pi/2$ total linear retardation at 1550 nm with the fast axis in the bend plane of the fiber; i.e., they act like quarter wave-plates. The azimuthal angles, θ_1 and θ_2, of these paddles are specified relative to a common arbitrary reference plane (i.e., the table). The remainder of the fiber constituting the laser cavity is mechanically secured so that the magnitude and principal axes of its birefringence (due to bends,

strain, splices, etc.) is constant. The magnitude of the residual birefringence (see below) can be determined and is found to be less than $\pi/4$; it is typically around $\pi/8$. The total cavity birefringence is dominated by the paddles and by adjusting θ_1 and θ_2, the retardance can be varied from 0 to slightly greater than 3 rad. Approximately 60% of the cavity fiber is contained in the paddles and these lengths are considerably shorter than the soliton period. Therefore, characterizing the total cavity retardance by its net value is justified.

The entire measurement apparatus, including the fiber laser, is shown in Fig. 6. It can determine if the pulses are evolving (and how rapidly) as they circulate in the cavity. For conditions where the polarization does not evolve, the azimuthal orientation of the principal axes in the cavity and the complete output polarization state can be determined. The measurement of the rate of polarization evolution is equivalent to measuring the cavity retardance.

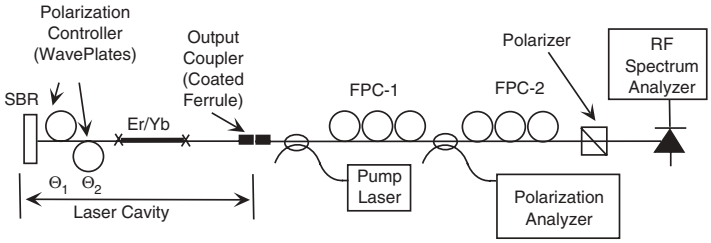

Fig. 6. Diagram of experiment used to observe polarization evolution in a mode-locked fiber laser

As the pulse circulates in the cavity, its polarization state evolves under the influence of the net (linear plus nonlinear) birefringence in the cavity. The polarization state is effectively sampled each time the pulse reflects off the output coupler. To measure the evolution of the polarization, the output is passed through a linear polarizer and the transmitted intensity is measured with a fast, polarization- insensitive photodiode. The linear polarizer maps the evolution of the polarization into amplitude modulation. The amplitude modulation is detected by measuring the radio-frequency (RF) spectrum of the signal emitted by the photodiode, and observing the frequencies of the resulting side-bands.

The RF spectrum consists of a series of spikes at integer multiples of the cavity repetition frequency. Each spike has upper and lower side-bands at relative frequency $\Delta = \gamma c/n\pi$, where n is the average index of refraction in the cavity. The product $\Delta\tau_c$, where τ_c is the round-trip time for the cavity, is the number of round trips required for the pulse to undergo a full polarization evolution and return to its original state, i.e., experience a total of 2π retardance. Hence the magnitude of the total round-trip cavity birefringence is $\beta = 2\pi\Delta\tau_c = 2l_c\gamma$ (in radians). From this ,we can see that measuring Δ is equivalent to measuring either β or γ. For a cavity birefringence of larger

than π, Δ is aliased to below $1/(2\tau_c)$, because the polarization is only sampled once per round trip. If the polarizer is aligned along either principal axis, the amplitude modulation is not present. Hence, the orientation of the cavity axes can be determined by rotating the polarizer until the side-bands vanish. However, this measurement does not determine which axis is fast and which is slow. See [38] for a derivation of the RF spectrum.

In circumstances where the polarization is not evolving, it is useful to have a complete characterization of the polarization state. This is obtained by using a commercial polarization state analyzer.

To be useful, the measurement of both the cavity axes and the complete polarization state need to be made on the light at the output coupler. Any birefringence in the fiber intervening between the output coupler and the measurement apparatus will change the polarization state. It is therefore necessary to use fiber polarization controllers to compensate the extra-cavity birefringence (FPC-1 and FPC-2 in Fig. 6) [27].

2.3 Results

The fundamental measurement is to determine the polarization evolution frequency, Δ, as a function of the angles θ_1 and θ_2 of the polarization controller paddles inside the laser cavity. Typical results are shown in Fig. 7.

As mentioned above, the measurement of Δ is equivalent to measuring the round trip retardance of the laser cavity. The overall structure of $\Delta(\theta_1, \theta_2)$ is well reproduced if the total cavity birefringence is calculated using a Jones vector formulation [25]. The retardance of the paddles and the

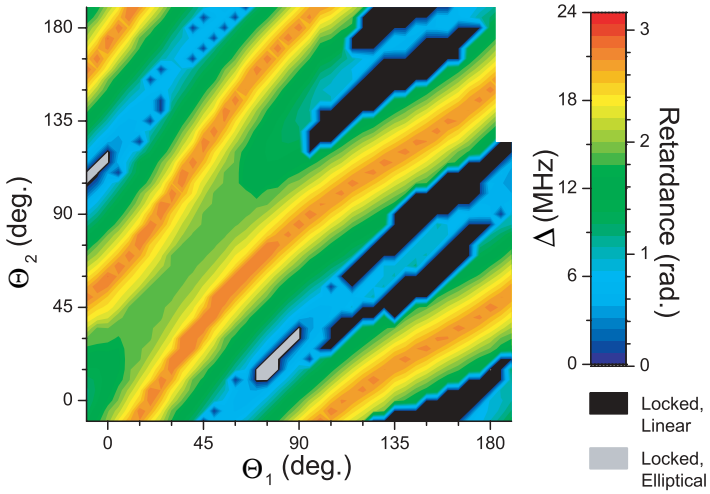

Fig. 7. The polarization evolution frequency, Δ, as a function of the azimuthal angles of the two intra-cavity paddles, θ_1 and θ_2

residual birefringence (retardance and axis orientation) used in the calculation are adjusted to obtain agreement with the data. The paddle retardance is found to be slightly under the design value of a quarter wave. The data shown in Fig. 7 are taken with the laser mode-locked; the overall structure of $\Delta(\theta_1, \theta_2)$ is identical if the SBR is replaced with a high-reflector so that the laser runs CW. This demonstrates that nonlinear birefringence is weak.

The side- bands in the RF spectrum disappear for certain values of intracavity birefringence. The lack of side-bands means that the polarization evolution has ceased. This occurs when the polarization is locked and is not evolving as the pulse circulates in the cavity. These regions of locked polarization are indicated in Fig. 7. The cavity still has net non-zero retardance, which is confirmed by making measurements of Δ when the laser is operating CW. The sizes of the regions of locked polarization are found to depend on pulse energy [38]. The pulse energy-dependent sizes and positions of the regions suggest that nonlinearity is responsible for the polarization locking. This is confirmed by the fact that locking is not observed when the laser is operating CW. As discussed above, there are two mechanisms that can lead to pulses with a fixed state of polarization: polarization-locked vector solitons and the fast axis instability. These are differentiated by their polarization; PLVS have elliptical polarization, while the axis instability results in linear polarization. Measurement of the polarization state in the locked regions shows that the region centered about zero retardance is elliptically-polarized, while those centered at finite values of retardance are linearly-polarized. Based on these observations, the elliptically- polarized regions are tentatively assigned to the formation of PLVS and the linearly-polarized regions to the fast axis instability.

The two optical spectra shown in Fig. 5 are for cases where the polarization is (a) unlocked and (b) locked. Comparison of these spectra is interesting because of the appearance of additional side-bands in the unlocked case (denoted by "P" in the figure). These side bands are caused by the periodic perturbation of the polarization. Their positions depend on the intra-cavity birefringence in an analogous fashion to Δ. The optical side-bands are due to phase matching of the radiation shed by the soliton as it adjusts to perturbations [35, 36]. It is believed that radiation shed due to random perturbation of the polarization will represent an ultimate limit in very high-speed soliton communication systems. The presence of these polarization-induced side-bands is direct evidence that the polarization perturbations do cause solitons to radiate.

To confirm that the polarization locked state with elliptical polarization is a PLVS, further measurements were performed (see [38]). As expected, the intensities along the principal axes are equal for zero birefringence, and increase linearly with increasing birefringence. The relative phase between the two components is found to be approximately constant at either $+\pi/2$ or $-\pi/2$. Both of these exactly match our prediction for how a PLVS maintains

stability. Additionally, the pulse energy dependence of the maximum retardance and relative optical bandwidths agree well with numerical simulations [28, 38]. Finally, it was observed that the locking is hysteretic with respect to the cavity birefringence, which again is consistent with the explanation of the locking mechanism.

To verify the origin of the locked regions with linear polarization, the polarization angle was measured as a function of θ_2. This agreed well with slow axis of the cavity as a function of θ_2, as expected if the fast axis is unstable. The boundaries of the linearly-locked region were also consistent with it being due to a slow axis instability.

2.4 Summary

The output of a mode-locked fiber laser can have a locked polarization state for certain settings of the intra-cavity birefringence. Extensive experiments examined the underlying physical mechanism. For very low values of birefringence, the output is elliptically-polarized and is due to the formation of polarization-locked vector solitons. For slightly larger retardance, the output is linearly-polarized and is assigned to the instability of the fast axis. Theoretical simulations provide good agreement with the experiment. Because the round trip gain and loss in the fiber laser is small, it provides a better approximation to a conservative system than that provided by a standard telecommunications long distance transmission system. It also provides and essentially infinite propagation distance.

3 Soliton Explosions

Dissipative systems display more complicated dynamics than integrable systems. These dynamics can have exquisite dependence on parameters. Examples include periodic or chaotic behavior or switching among stable states. In certain situations, simulations show that solitons undergo dramatic transients and then return to the initial conditions [39]. These transients have been dubbed "exploding solitons" [40]. During an explosion, the soliton energy and spectrum undergo dramatic changes, but return to the steady state value afterwards. The existence of such instabilities may influence the design of long-distance communications systems and ultra-fast mode-locked lasers. Such transients are detrimental to either application. System design that avoids them requires knowledge that they exist and accurate, experimentally-verified models.

Capturing a transient event, such as an exploding soliton, is challenging. As mentioned above, mode-locked lasers provide the ability to continuously monitor the evolution of a soliton as it circulates. This facilitates capturing rare events. The explosions last for approximately 10 μs, which corresponds to a few hundred round trips.

3.1 Experiment

Soliton explosions are detected by temporally recording the output spectrum of the laser and the integrated energy of the pulse. Full characterization by a technique such as frequency-resolved optical gating [41] would be preferable. However, all such techniques utilize optical nonlinearities and cannot make single shot measurements on the nano-joule pulses that are directly produced by a mode-locked oscillator. Thus, measurement of the temporally-resolved spectrum is the only technique that can provide information about the pulse dynamics on timescales comparable to the round-trip time of the laser cavity.

Figure 8 shows the experimental setup. The laser has a "stretched" cavity that is 4 times longer than typical (40 ns roundtrip time). The laser spectrum shows strong resonant side-bands from phase-matching of the dispersive waves shed as the 50 fs soliton undergoes periodic perturbation [35, 36]. These are stronger than typically observed in a Kerr-lens mode-locked (KLM) laser, due to the stretched cavity and lack of spectral filtering. The gain bandwidth is broader than the pulse spectrum and is limited by the mirror reflectivity. The use of a stretched cavity is crucial, because it means that the pulse spectrum is dominated by soliton dynamics through side-band formation, rather than through explicit spectral filtering due to a tuning element or mirror reflectivity. This is because the frequency spacing of the side-bands is inversely proportional to cavity length. The output of the laser is spectrally dispersed by a diffraction grating across an array of six detectors. The spectral dispersion is adjusted so that each channel has a spectral width of ∼12 nm (full-width half- maximum). The data from all of the channels are synchronously recorded with an electronic bandwidth corresponding to averaging over approximately five successive pulses.

The spectrally-integrated intensity (i.e., total pulse energy) is also synchronously recorded on a separate channel. An optical spectrum analyzer is used to record the steady-state spectrum. The six channels are positioned on

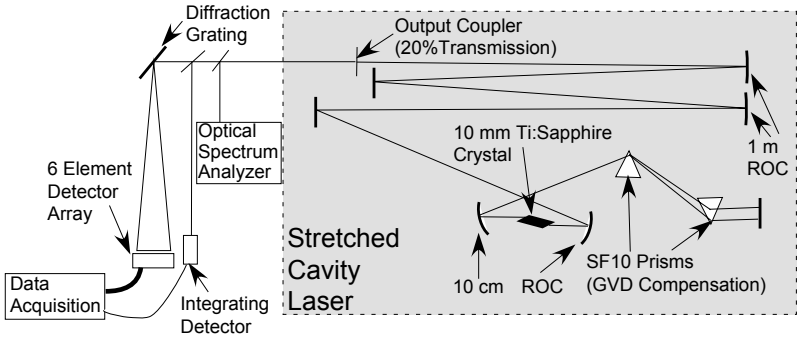

Fig. 8. Experimental set-up for observing exploding solitons. The radii of curvature (ROC) of the laser mirrors are indicated; those not designated are flat

the short wavelength side of the steady state spectrum, because the spectral transients occur in that direction. This was verified by running the optical spectrum analyzer in "peak hold" mode during a large number of explosions, capturing the highest intensity at a given wavelength. The long wavelength side of the captured spectrum was identical to the steady state spectrum. A typical steady- state spectrum and the spectral response of the individual channels are shown in Fig. 9.

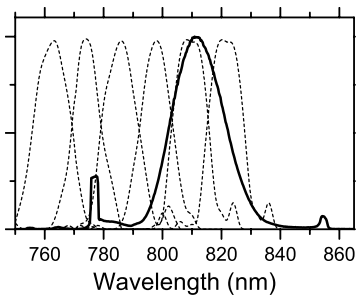

Fig. 9. Typical steady-state output spectrum of the laser and the spectral response of each of the channels (*dashed*)

3.2 Results

Data exhibiting a typical soliton explosion are shown in Fig. 10. The bulk of the integrated spectrum is concentrated around the central frequency of 812 nm. When an explosion occurs, the spectrum becomes asymmetric, abruptly blue shifts and subsequently returns to the original position. This can occur as either an isolated event, as shown in Fig. 10a, or in a burst, as shown in Fig. 10b. The intra-cavity dispersion controls which of these occurs. Small oscillations that slowly increase in amplitude precede an explosion and slowly die out after the explosion. Time-averaged auto-correlations show that the steady-state pulse is the same before and after an explosion, and a transform-limited pulse can be obtained with external dispersion compensation. This fact, together with the observation that the pulse spectrum *narrows* during the explosion, is proof that the pulse becomes longer in time, as predicted [39], because of the Fourier transform limit.

Typical measured intra-cavity dispersion, corresponding to the data in Fig. 10, is shown in Fig. 11. Measurements were performed in situ by measuring the repetition rate as a function of wavelength [42]. The change in slope and curvature show that higher-order dispersion is present and that it changes between the two cases, making it difficult to get a simple quantitative assessment of the change in dispersion.

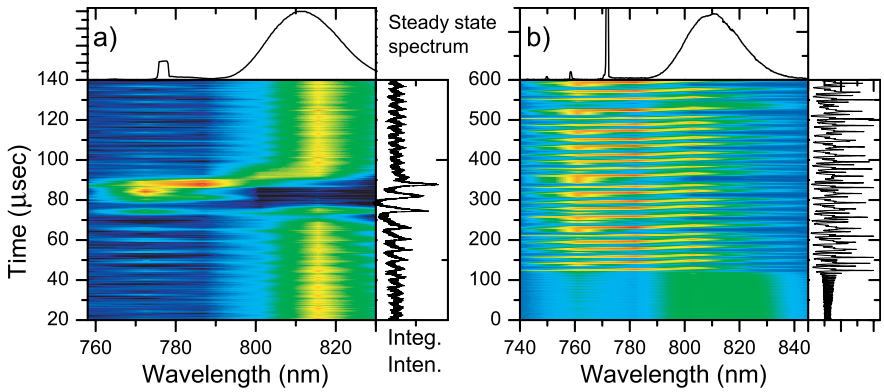

Fig. 10. Typical data showing soliton explosions. In (**a**) the dispersion is adjusted to yield solitary explosions, while in (**b**) it is adjusted to yield bursts. The resolution and positions of the spectral channels has been optimized in (**b**). The *upper* panel in each case shows the steady-state spectrum for reference. The *right* panels show the output of the spectrally-integrated detector

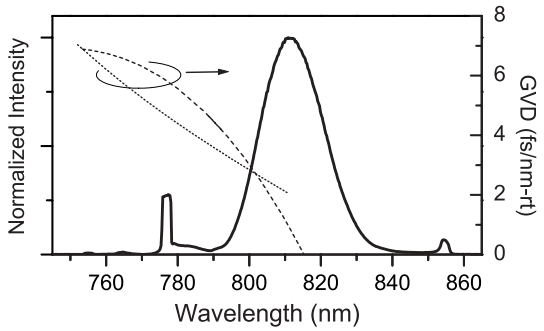

Fig. 11. Measured intra-cavity dispersion corresponding to Fig. 10(**a**) (*dotted*) and (**b**) (*dashed*). The *solid* line shows the steady-state laser spectrum for reference

The rate at which explosions occur can be controlled by changing the pump power, as this determines the steady-state soliton energy. The range of pump powers for which explosions occur depends on the intra-cavity dispersion. A histogram of the frequency of the time between spontaneously-occurring explosions (called the "laminar time" because intermittency was first studied in the context of the onset of turbulence) shows a power-law dependence, with $P(\tau) \sim \tau^{-1}$ (Fig. 12). Strong external perturbations, such as a sharp rap on the laser, can trigger an explosion if the pump power is in the range for which explosions occur. No correlations with typical vibrations in the laboratory are observed. Thus the explosions are not simply due to technical noise. Although the onset of the explosions is not our focus here,

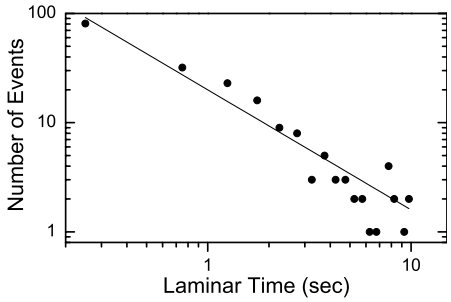

Fig. 12. Histogram of the number of events as function of the time between events ("Laminar time"). Line is a fit to a power-law with an exponent of 1.1

power-law behavior in the frequency of laminar times is a signature of "intermittency" in a system exhibiting chaotic dynamics [43].

The bursts of explosions, as seen in Fig. 10b, on average last for 0.95 ms [for the same intra-cavity dispersion as Fig. 10b]. However, a histogram of burst lengths [see Fig. 13] shows a minimum duration of around 0.4 ms and a general decrease in the number with increasing length.

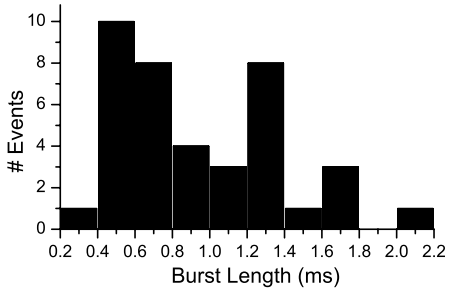

Fig. 13. Histogram of the length of bursts such as is seen in Fig. 10b

If explicit spectral filtering is imposed on the laser, explosions do not occur. Instead, strong oscillations eventually break out at pump powers lower than those characteristic of the occurrence of explosions. We attribute these oscillations to relaxation phenomena, because the damping time of relaxation oscillations increases as the pump power is lowered towards the lasing threshold [1]. The oscillations are distinct from explosions in that the large abrupt change in center wavelength does not occur; on the contrary, the center wavelength is constant, and only the width and pulse energy oscillate.

3.3 Summary

The experimentally-observed features are similar to those predicted theoretically in the continuous model [39]. However, the real system is not continuous. The discreteness of the laser must be taken into account to verify that the predictions still hold. Including the discreteness of the actual laser does not change the results qualitatively [40]. The asymmetry of the experimentally-observed explosions is reproduced in the calculations when higher-order dispersion is included. This is because higher-order dispersion breaks the symmetry between higher and lower frequencies.

In summary, the following features are observed: (1) explosions occur occasionally; (2) the rate is sensitive to pump power; (3) the laser is close to the mode-locking threshold; (4) the explosions are similar, but not identical; (5) an explosion can occur spontaneously, but can also be triggered by external perturbations; (6) there is no precursor to an explosion. Similar features are observed in the simulations.

4 Carrier-Envelope Phase

Over the last few years, one of the most exciting developments in mode-locked lasers has been the ability to stabilize the carrier-envelope phase of the output pulses [44, 45, 46]. The electric field of a pulse, $E(t)$, can be written

$$E(t) = \hat{E}(t)\mathrm{e}^{\mathrm{i}(\omega t+\phi_{CE})} \tag{6}$$

where $\hat{E}(t)$ is the "slowly" varying envelope that is superimposed on a carrier wave oscillating at a frequency ω. The phase between the carrier and envelope is designated by ϕ_{CE}, as shown in Fig. 14. Note that 6 can only be used when the duration of $\hat{E}(t)$ is greater than that of a single cycle of the carrier wave, otherwise it no longer describes a propagating solution to

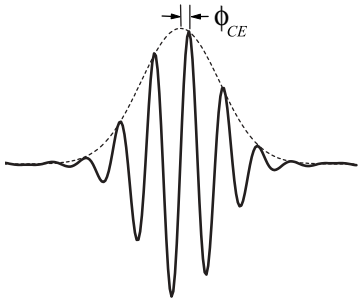

Fig. 14. The electric field of a few-cycle pulse showing the definition of the carrier-envelope phase, ϕ_{CE}. The *dashed* line shows the envelope

Maxwell's equations. For more complex waveforms, there is ambiguity in the decomposition into carrier and envelope. However, in practical situations, it is usually clear how to do it.

Normally in optics, the overall phase of the electric field is irrelevant, because measurements are always made of intensity, not of the field itself. Only relative phases, for example between beams traversing the two arms of an interferometer, matter. However, the ability to measure ϕ_{CE} overcomes this, and will allow the optical phase to be measured relative to the pulse envelope, the phase of which can in turn be measured relative to an arbitrary radio-frequency clock signal. The optical phase becomes relevant in extreme nonlinear optics, where processes occur which are sensitive to the electric field of the pulse, rather than the intensity [47]. By simply stabilizing ϕ_{CE}, the frequency spectrum can be controlled, and this has dramatically simplified optical frequency metrology [44, 48, 49] and optical atomic clocks [50, 51].

This advance makes the phase dynamics of the intra-cavity pulse a subject of strong interest. Heretofore, the phase evolution of solitons has largely been ignored, in no small part because it was not relevant to experiments. Thus the phase dynamics of solitons is now becoming a topic of interest.

4.1 Frequency Domain Stabilization of ϕ_{CE}

The difference between group and phase velocities inside the cavity of a mode-locked laser causes ϕ_{CE} to evolve on a pulse-to-pulse basis, as shown in Fig. 15a. The pulse-to-pulse change is designated $\Delta\phi_{CE}$ and is given by

$$\Delta\phi_{CE} = \frac{\omega_c v_g}{f_{rep}} \left(\frac{1}{v_g} - \frac{1}{v_p} \right) , \tag{7}$$

where ω_c is the carrier frequency, f_{rep} is the repetition rate, v_g is the intra-cavity group velocity and v_p is the intra-cavity phase velocity. Stabilization of ϕ_{CE} means controlling $\Delta\phi_{CE}$, with the simplest case being $\Delta\phi_{CE} = 0$, which means that all of the pulses have identical ϕ_{CE}, although its actual value is unknown.

The evolution of ϕ_{CE} is measured in the frequency domain. The spectrum of a pulse train is a comb of discrete lines separated by f_{rep}. If the pulses are all identical, the frequencies of the comb lines are simply integer multiples of f_{rep}. However, evolution of ϕ_{CE} causes a rigid shift of the comb by an amount

$$f_0 = \Delta\phi_{CE} f_{rep}/2\pi \ . \tag{8}$$

Thus the optical frequency of comb line n is $\nu_n = n f_{rep} + f_0$. This correspondence between time and frequency is shown in Fig. 15. (For a full derivation, see [46].) Measurement of $\Delta\phi_{CE}$ is actually implemented by measuring f_0 using a "self-referencing" technique [44, 52]. In self-referencing, comb line n is frequency-doubled and then heterodyned with comb line $2n$. Heterodyning yields the frequency difference, $2\nu_n - \nu_{2n} = 2(n f_{rep} + f_0) - (2n f_{rep} + f_0) = f_0$.

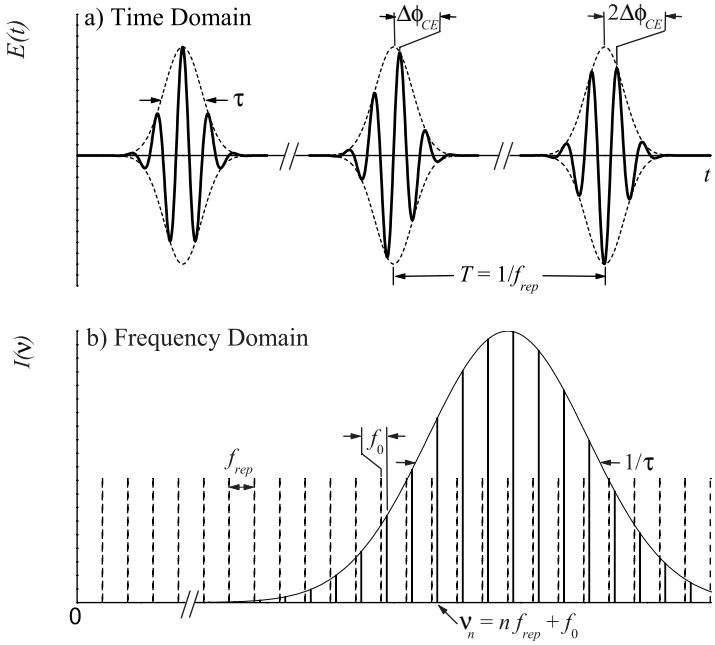

Fig. 15. Diagram showing (**a**) the time domain picture of a pulse train including evolution of ϕ_{CE} , and (**b**) the frequency spectrum showing the offset frequency f_0

4.2 Time-Domain Measurement of $\Delta\phi_{CE}$

A cross-correlator is used to perform time-domain measurement of the evolution of the carrier envelope phase [44, 53]. A cross-correlator consists of a Michelson interferometer followed by nonlinear detection (see Fig. 16). To obtain a cross-correlation between successive pulses emitted by the laser, one arm of the interferometer includes a delay that corresponds to the round trip time of the laser cavity (for the specific case shown here, it is actually two round trip times, so the correlation between pulse i and pulse $i + 2$ is actually obtained). In the absence of nonlinear detection, a field correlation is obtained; this is just the Fourier transform of the spectrum and it cannot distinguish between a short pulse and broad-band white light. The nonlinear interferogram that is obtained by using a detection scheme that includes a second-order nonlinearity clearly distinguishes between these cases and can provide information about pulse characteristics. Because air has significant dispersion for ultra-short pulses, the interferometer must be in an evacuated enclosure.

Two typical interferograms are shown in Fig. 16b. If the pulses were identical, i.e., $\Delta\phi_{CE} = 0$, then the interferograms would be perfectly symmetric. The presence of a pulse-to-pulse phase shift means the interference fringes are shifted with respect to the overall envelope, thus breaking the symmetry.

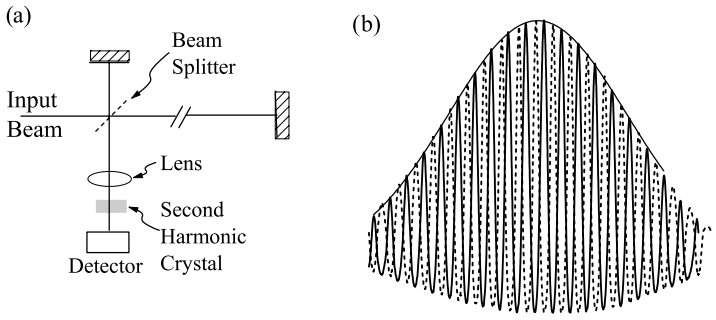

Fig. 16. (**a**) Schematic of a cross-correlator for measuring pulse-to-pulse phase shift. (**b**) Results showing stabilization of the pulse-to-pulse phase shift for two cases differing by $\sim\pi$

To aid in visualizing and extracting the phase of the fringes, the black line shows a fit to the peaks of the fringes. The two instances shown in Fig. 16b correspond to changing f_0 by $f_{rep}/2$, which clearly yields the expected π shift in the fringes. Systematically varying f_0 yields exactly the change in $\Delta\phi_{CE}$ predicted by 8.

4.3 Phase-Intensity Dynamics

These advances make it possible to study the phase dynamics of the circulating pulse in ways there have not previously been possible. The most interesting aspect of this is how phase evolution depends on the pulse intensity. From a fundamental point-of-view, this is interesting because it arises from a complex interplay between nonlinearity and dispersion, the key ingredients in any soliton system. But it is also of great practical importance because it couples intensity fluctuations into phase fluctuations. This can be detrimental, but can also be put to use by actively controlling the pump power, thereby controlling the phase evolution.

One of the early papers on carrier-envelope phase evolution by Xu et al. [53] noticed that $\Delta\phi_{CE}$ depended on the pump power, which in turn controls the pulse intensity. A simple analysis considered the pulse as a soliton, but yielded the opposite sign for $\partial\Delta\phi_{CE}/\partial I$, where I is the intensity, compared to the experiment. This analysis only included the fact that the phase velocity is intensity-dependent because of the Kerr effect. The discrepancy between theory and experiment was attributed to the fact that, in the experiment, there was a spectral shift with intensity, which, coupled with group velocity dispersion, gives a large contribution to $\partial\Delta\phi_{CE}/\partial I$ with the opposite sign from the expected nonlinear contribution. The empirical observation was sufficient to enable the use this effect for controlling $\Delta\phi_{CE}$ [54].

A subsequent analysis included the fact that the group velocity also is intensity-dependent (often called the "shock" term) [55]. This work found

that the nonlinear change of the group velocity was larger than the nonlinear change in the phase velocity, which predicts the opposite sign change in $\partial\Delta\phi_{CE}/\partial I$, as compared with the previous analysis.

More recent careful experiments show that both signs $\partial\Delta\phi_{CE}/\partial I$ can actually occur [56]. Careful measurements of the spectral shift show that it behaves in a similar fashion, turning around at approximately the same intensity as does f_0. Furthermore, this work showed that $\partial\Delta\phi_{CE}/\partial I$ depends on the pulse width. Specifically, for very short pulses, with very large spectral bandwidth, $\partial\Delta\phi_{CE}/\partial I$ tends to be small. This is consistent with spectral shifts being important; for very short pulses, the spectrum is so wide that it is prevented from shifting due to implicit spectral filtering by various intracavity elements.

A different theoretical approach is to numerically solve Maxwell's equations. Such a direct solution avoids the approximations made in deriving the NLSE, although it is computationally more difficult and does not permit analysis. The results confirm the soliton analysis at low intensities. However, at high intensities, pulse reshaping can become appreciable and effectively change the sign of $\partial\Delta\phi_{CE}/\partial I$ [57]. This is accompanied by spectral shifts, however it occurs over much larger changes in intensity than observed in the experiments.

A complete understanding of the intra-cavity phase dynamics of a mode-locked laser has not been obtained so far. A complete analysis, for example including the dispersion map, should provide better insight.

5 Summary

Hopefully, this chapter has shown that mode-locked lasers are a very interesting "playground" for temporal solitons. Specifically, they provide a means for observing phenomena that are hard to observe in other systems. This can be due to the fact the evolution must be carefully monitored over long times, or because of the occurrence of infrequent events that are difficult to capture. This is a two-way street, since the lasers provide a test-bed for soliton dynamics, but at the same time the soliton theory helps to improve the operation of the lasers.

Acknowledgements

The author would like to thank Nail Akhmediev and Jose Soto-Crespo for stimulating discussions regarding the work in Sects. 2 and 3. In addition, contributions by Brandon Collings, Wayne Knox and Keren Bergman to the experiments presented in Sect. 2 are gratefully acknowledged. Contributions by David Jones, Tara Fortier, Jun Ye and John Hall to Sect. 4 are gratefully acknowledged.

References

1. For a textbook-level discussion of lasers, see for example A. E. Siegman, *Lasers* (University Science Books, Mill Valley, 1986) or J. T. Verdeyen, *Laser Electronics* (Prentice-Hall, Englewood Cliffs, 1995). 184, 199
2. E. P. Ippen, Appl. Phys. B **58**, 159 (1994). 185
3. Y. Chen, F. X. Kärtner, U. Morgner, S. H. Cho, H. A. Haus, E. P. Ippen, J. G. Fujimoto, J. Opt. Soc. Am. B **16**, 1999 (1999). 185
4. E. Desurvire, *Erbium-Doped Fiber Amplifiers* (John Wiley & Sons, New York, 1994). 185
5. B. C. Collings, K. Bergman, S. T. Cundiff, S. Tsuda, J. N. Kutz, J. E. Cunningham, W. Y. Jan, M. Koch, W. H. Knox, IEEE J. Sel. Top. Quantum Electr. **3**, 1065 (1997). 186
6. L. E. Nelson, D. J. Jones, K. Tamura, H. A. Haus, E. P. Ippen, Appl. Phys. B **65**, 277 (1997). 186
7. A. Hasegawa, F. Tappert, Appl. Phys. Lett. **23**, 142 (1973). 186
8. I. P. Kaminow, IEEE J. Quantum Electron. **17**, 15 (1981). 186
9. L. F. Mollenauer, R. H. Stolen, J. P. Gordon, Phys. Rev. Lett. **45**, 1095 (1980). 186
10. H. A. Haus, W. S. Wong, Rev. Mod. Phys. **68**, 423 (1996). 186
11. C.D. Poole, J. Nagel, Polarization effects in lightwave systems. In: *Optical Fiber Telecommunications IIIA*, ed. by I. P. Kaminow, T. L. Koch (Academic, San Dieogo 1997) p. 114. 186, 189
12. M. N. Islam, C. D. Poole, J. P. Gordon, Opt. Lett. **14**, 1011 (1989). 186
13. C. R. Menyuk, Opt. Lett. **12**, 614 (1987); IEEE J. Quantum Electron. **23**, 174 (1987); J. Opt. Soc. Am. B **5**, 392 (1988). 187, 188, 189
14. D. N. Christodoulides, R. I. Joseph, Opt. Lett. **13**, 53 (1988). 187, 189
15. S. T. Cundiff, B. C. Collings, N. N. Akhmediev, J. M. Soto-Crespo, K. Bergman, W. H. Knox, Phys. Rev. Lett. **82**, 3988 (1999). 187, 188
16. M. V. Tratnik, J. E. Sipe, Phys. Rev. A **38**, 2011 (1988). 187, 188, 189
17. N. Akhmediev, A. Buryak, J. M. Soto-Crespo, Opt. Commun. **112**, 278 (1994). 187, 188, 190
18. N. Akhmediev, J. M. Soto-Crespo, Phys. Rev. E **49**, 5742 (1994). 187, 188, 189, 190
19. N. N. Akhmediev, A. V. Buryak, J. M. Soto-Crespo, D. R. Andersen, J. Opt. Soc. Am. B **12**, 434 (1995). 187, 188, 189
20. J. M. Soto-Crespo, N. Akhmediev, A. Ankiewicz, Phys. Rev. E **51**, 3547 (1995). 187, 188, 189
21. Y. Chen, J. Atai, J. Opt. Soc. Am. B **12**, 434 (1995). 187, 188
22. H. G. Winful, Opt. Lett. **11**, 33 (1986). 187, 190
23. K. J. Blow, N. J. Doran, D. Wood, Opt. Lett. **12**, 202 (1987). 187, 189, 190
24. Y. Barad, Y. Silberberg, Phys. Rev. Lett. **78**, 3290 (1997). 187
25. S. T. Cundiff, B. C. Collings, W. H. Knox, Optics Express **1**, 12 (1997). 188, 193
26. N. N. Akhmediev, J. M. Soto-Crespo, S. T. Cundiff, B. C. Collings, W. H. Knox, Opt. Lett. **23**, 852 (1998). 188
27. B. C. Collings, S. T. Cundiff, N. N. Akhmediev, J. M. Soto-Crespo, K. Bergman, W. H. Knox, J. Opt. Soc. Am. B **17**, 354 (2000). 188, 193
28. J. M. Soto-Crespo, N. N. Akhmediev, B. C. Collings, S. T. Cundiff, K. Bergman, W. H. Knox, J. Opt. Soc. Am. B **17**, 366 (2000). 188, 195
29. G. P. Agrawal, *Nonlinear Fiber Optics* (Academic Press, San Diego 1995). 188, 191
30. N. N. Akhmediev and A. Ankiewicz, *Solitons: Nonlinear pulses and beams*, (Chapman & Hall, London 1997). 188
31. S.V. Manakov, Sov. JETP **38**, 248 (1974). 188

32. J. U. Kang, G. I. Stegeman, J. S. Aitchison, N. Akhmediev, Phys. Rev. Lett. **76**, 3699 (1996). 188
33. S. G. Evangelides, L. F. Mollenauer, J. P. Gordon, N. S. Bergano, J. Lightwave Technol. **10**, 28 (1992). 189
34. L. F. Mollenauer, K. Smith, J. P. Gordon, C. R. Menyuk, Opt. Lett. **14**, 1219 (1989). 189
35. S. M. J. Kelley, Electron. Lett. **28**, 806 (1992). 191, 194, 196
36. J. P. Gordon, J. Opt. Soc. Am. B **9**, 91, (1992). 191, 194, 196
37. H. C. Lefevre, Electron. Lett. **16**, 778 (1980). 191
38. S. T. Cundiff, B. C. Collings, K. Bergman, CHAOS **10**, 613 (2000). 193, 194, 195
39. J. M. Soto-Crespo, N. Akhmediev, A. Ankiewicz, Phys. Rev. Lett. **85**, 2937 (2000). 195, 197, 200
40. S. T. Cundiff, J. M. Soto-Crespo N. N. Akhmediev, Phys. Rev. Lett. **88**, 073903 (2002). 195, 200
41. R. Trebino, *Frequency-Resolved Optical Gating: the Measurement of Ultrashort Laser Pulses* (Kluwer, Boston 2002). 196
42. W. H. Knox, Opt. Lett. **17**, 514 (1992). 197
43. H. G. Schuster, *Deterministic Chaos*, 3rd ed. (VCH, Weinheim 1995). 199
44. D. J. Jones, S. A. Diddams, J. K. Ranka, A. Stentz, R. S. Windeler, J. L. Hall, S. T. Cundiff, Science **288**, 635 (2000). 200, 201, 202
45. A. Apolonski, A. Poppe, G. Tempea, C. Spielmann, T. Udem, R. Holzwarth, T. W. Hänsch, F. Krausz: Phys. Rev. Lett. **85**, 740 (2000). 200
46. S. T. Cundiff, J. Phys. D **35**, R43 (2002). 200, 201
47. A. Baltuška, T. Udem, M. Uiberacker, M. Hentschel, E. Goulielmakis, C. Gohle, R. Holzwarth, V. S. Yakoviev, A. Scrinzi, T. W. Hänsch, and F. Krausz, Nature **421**, 611 (2003). 201
48. S. A. Diddams, D. J. Jones, J. Ye, T. Cundiff, J. L. Hall, J. K. Ranka, R. S. Windeler, R. Holzwarth, T. Udem, and T. W. Hänsch, Phys. Rev. Lett. **84**, 5102 (2000). 201
49. S. T. Cundiff, J. Ye, Rev. Mod. Phys. **75**, 325 (2003). 201
50. S. A. Diddams, T. Udem, J. C. Bergquist, E. A. Curtis, R. E. Drullinger, L. Hollberg, W. M. Itano, W. D. Lee, C. W. Oates, K. R. Vogel, D. J. Wineland, Science **293**, 825 (2001). 201
51. J. Ye, L.-S. Ma, J. L. Hall, Phys. Rev. Lett. **87**, 270801 (2001). 201
52. H. R. Telle, G. Steinmeyer, A. E. Dunlop, J. Stenger, D. H. Sutter, U. Keller, Appl. Phys. B **69**, 327 (1999). 201
53. L. Xu, C. Spielmann, A. Poppe, T. Brabec, F. Krausz, and T. W. Hänsch, Opt. Lett. **21**, 2008 (1996). 202, 203
54. A. Poppe, R. Holzwarth, A. Apolonski, G. Tempea, C. Spielmann, T. W. Hänsch, F. Krausz, Appl. Phys. B **72**, 977. (2001). 203
55. H. A. Haus, E. P. Ippen, Opt. Lett. **26**, 1654 (2001). 203
56. K. W. Holman, R. J. Jones, A. Marian, S. T. Cundiff, J. Ye, Opt. Lett. **28**, 851 (2003). 204
57. P. Goorjian, S.T. Cundiff, Opt. Lett. **29**, 1363 (2004). 204